Elementary Computation of Object Approach by a Wide-Field Visual Neuron

Nicholas Hatsopoulos; Fabrizio Gabbiani; Gilles Laurent

Science is currently published by American Association for the Advancement of Science.

came apparent that at least one residue, Val[65], did not fit the electron density well in either solvent-flattened or model-phased $2F_o - F_c$ maps. This observation and an inconsistent subunit mass determined by triple quadropole electrospray mass spectrometry led us to resequence the plasmid DNA that had been used to overexpress LpxA. Discrepancies with the published DNA sequence corresponding to three altered amino acids were detected: Ser[64]→Gln, Val[65]→Phe, and Asp[125]→His (3). The new sequence is consistent with a derived subunit mass of 28,081 mass units, in agreement with the 28,083 ± 3 mass unit value determined by mass spectrometry (29).

10. We define residues that participate in β strands as those with main-chain ϕ, Ψ angles that are characteristic of ordinary β structures and that form interstrand hydrogen bonds with backbone amide and carbonyl groups.
11. J. S. Richardson, *Adv. Protein Chem.* **34**, 167 (1981).
12. M. S. Anderson *et al.*, *J. Biol. Chem.* **268**, 19858 (1993).
13. M. D. Yoder and F. Jurnak, *FASEB J.* **9**, 335 (1995).
14. M. D. Yoder, N. T. Keen, F. Jurnak, *Science* **260**, 1503 (1993).
15. M. D. Yoder, S. E. Lietzke, F. Jurnak, *Structure* **1**, 241 (1993).
16. R. Pickersgill, J. Jenkins, G. Harris, W. Nasser, J. Robert-Baudouy, *Nature Struct. Biol.* **1**, 717 (1994).
17. S. Steinbacher *et al.*, *Science* **265**, 383 (1994).
18. J. S. Richardson, *Proc. Natl. Acad. Sci. U.S.A.* **73**, 2619 (1976).
19. K. Nagano, *J. Mol. Biol.* **109**, 235 (1977).
20. C. Chothia, *ibid.* **75**, 295 (1973).
21. M. J. E. Sternberg and J. M. Thornton, *ibid.* **110**, 269 (1977).
22. K.-C. Chou, G. Nemethy, M. Pottle, H. A. Scheraga, *ibid.* **205**, 241 (1987).
23. D. N. Crowell, M. S. Anderson, C. R. H. Raetz, *J. Bacteriol.* **168**, 152 (1986).
24. U. Pfitzner, C. R. H. Raetz, S. L. Roderick, *Proteins Struct. Funct. Genet.* **22**, 191 (1995).
25. W. Kabsch, *J. Appl. Crystallogr.* **21**, 916 (1988).
26. W. Furey and S. Swaminathan, *American Crystallographic Association Meeting Summaries* (abstr.), 73 (1995).
27. A. T. Brunger, A. Krukowski, J. W. Erickson, *Acta Crystallogr.* **A46**, 585 (1990).
28. D. E. Tronrud, L. F. Ten Eyck, B. W. Matthews, *ibid.* **A43**, 489 (1987).
29. C. R. H. Raetz and S. L. Roderick, data not shown.
30. S. V. Evans, *J. Mol. Graphics* **11**, 134 (1993).
31. We gratefully acknowledge U. Pfitzner for technical assistance, R. Zheng for aid in DNA sequencing work, X.-J. Tang of the Albert Einstein College of Medicine Laboratory for Macromolecular Analysis for mass spectrometry, and M. Anderson, J. Blanchard, M. Degano, and G. Scapin for many helpful discussions. Supported in part by National Institutes of Health grants GM51310 (to C.R.H.R.) and AI38328 (to S.L.R.).

Elementary Computation of Object Approach by a Wide-Field Visual Neuron

Nicholas Hatsopoulos,* Fabrizio Gabbiani, Gilles Laurent†

An essential function of the brain is to detect threats, such as those posed by objects or predators on a collision course. A wide-field, movement-sensitive visual neuron in the brain of the locust was studied by presenting simulated approaching, receding, and translating objects. The neuron's responses could be described simply by multiplying the velocity of the image edge ($d\theta/dt$) with an exponential function of the size of the object's image on the retina ($e^{-\alpha\theta}$). Because this product peaks before the image reaches its maximum size during approach, this neuron can anticipate collision. The neuron's activity peaks approximately when the approaching object reaches a certain angular size. Because this neuron receives distinct inputs about image size and velocity, the dendritic tree of a single neuron may function as a biophysical device that can carry out a multiplication of two independent input signals.

Vision plays an important role in notifying animals of imminent danger, such as an impending collision with a predator or an environmental surface. One possible strategy for collision avoidance is for the animal to react when the object is at a given distance away from it. This would require that the animal estimate depth, using cues such as motion or binocular parallax. Many animals, such as arthropods, can avoid rapidly approaching objects, but are unlikely to use this strategy because their binocular fields and the spacing between their eyes are too small.

A second possible strategy is to react at a given time before collision by monitoring the symmetrical expansion of the image projected on the retina by the approaching object (1). Behavioral and electrophysiological evidence from birds and flies support the use of this strategy (2). Imagine an object subtending an angle θ at a distance *d* from the eye (Fig. 1A). If this object moves toward

California Institute of Technology, Biology Division, Pasadena, CA 91125, USA.

*Present address: Department of Neuroscience, Brown University, Providence, RI 02912, USA.
†To whom correspondence should be addressed. E-mail: laurentg@starbase1.caltech.edu

the animal at a constant velocity *v*, its image on the retina will grow increasingly faster as the object approaches (θ̇ will increase nonlinearly as θ increases; the dot means time derivative). The tau function (3),

$$\tau(t) = \frac{d}{\dot{d}} = \frac{\sin\theta\cos\theta}{\dot{\theta}} \approx \frac{\theta}{\dot{\theta}} \text{ if } \theta \text{ small}$$

where *t* is time, is useful because it can provide the time before collision without any explicit knowledge of *d*. The tau function can be obtained from the optical flow field and requires only knowledge of θ and θ̇, which can both be determined monocularly at the retina. The function τ(*t*) (4) could be encoded in the firing rate of a neuron, and an escape command would be triggered when τ(*t*) has decreased to below a threshold value (Fig. 1C). Alternatively, the brain could compute 1/τ(*t*), which peaks at collision (Fig. 1C). In this case, an escape command would be triggered when 1/τ(*t*) exceeds a certain threshold. In either case, the timing of escape depends on determining that a threshold has been crossed, which is a difficult problem for biological systems. We now report that a pair of identified neurons

in an insect brain adopts yet a different strategy to track object approach, combining θ and θ̇ nonlinearly to yield a response profile similar to the function *f*(*t*) (Fig. 1C).

We studied the LGMD and DCMD neurons (Fig. 1B), two connected, motion-sensitive neurons in the brain of the locust *Schistocerca americana* (5–7). These visual neurons respond to novel, small contrasting object motion, regardless of direction or orientation, and are inhibited by large-field motion (such as flow fields generated by the animal's own motion) (8). More recent investigations (9, 10) have shown that the LGMD and DCMD neurons respond preferentially to approaching rather than translating objects and have suggested that the feature most closely correlated with their firing is angular acceleration of the image edges (11).

We recorded the response of DCMD to simulated "approaching" objects presented monocularly to the animal (12) and noted that it differs significantly from the acceleration profile of the image. First, when a simulated object approached the animal at low but constant velocity (a condition in which image angular velocity and acceleration increase as the image grows larger), DCMD activity peaked before the image acceleration was maximal (Fig. 2A) (13). If DCMD tracked image acceleration, its firing rate should not decrease before the acceleration peak (14). The timing of the DCMD peak firing rate was strongly correlated with the collision time (Fig. 2C, regression coefficient = 0.963, r^2 = 0.9998) (15). The delay between peak firing and collision, however, was a function of both object size and object velocity (Fig. 2D). This indicates that DCMD does not encode τ(*t*) [or 1/τ(*t*)], because τ is independent of these two parameters. Second, when the simulated object decelerated while approaching the animal (image angular velocity held constant, that is, image acceleration θ̈ = 0), DCMD responded strongly at first and continued firing, although progressively less strongly, as the simulated object

"approached" (Fig. 2B). If DCMD were encoding image edge acceleration, it might have responded briefly when the object became detectable but should not have continued to respond during approach when the angular acceleration was zero. DCMD, therefore, does not appear to track image edge acceleration (16).

DCMD might rather implement an alternative representation of object approach such as that modeled by $f(t)$ [compare $f(t)$ (Fig. 1C) to DCMD response (Fig. 2A)]. Because θ (image size) and $\dot{\theta}$ (angular velocity) are both measured at the retina, we looked for a function of these two variables that reproduced the essential features of $f(t)$ (Fig. 1C). We first examined the dependence of DCMD activity on θ. If an object, a striped pattern, or a sine wave grating is moved laterally (translated) in front of the eye (rather than in depth), the response of DCMD is greater if the stimulus subtends a small angle (8). We studied the response of DCMD to squares of various sizes moving to the left or to the right, at either of two edge velocities (Fig. 2, E and F). We used constant edge velocity stimuli (17) so as not to confound the response with changing angular velocity signals. We observed that the firing rate of DCMD was well fitted by an
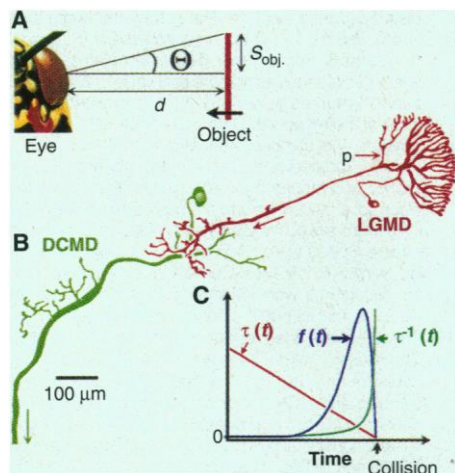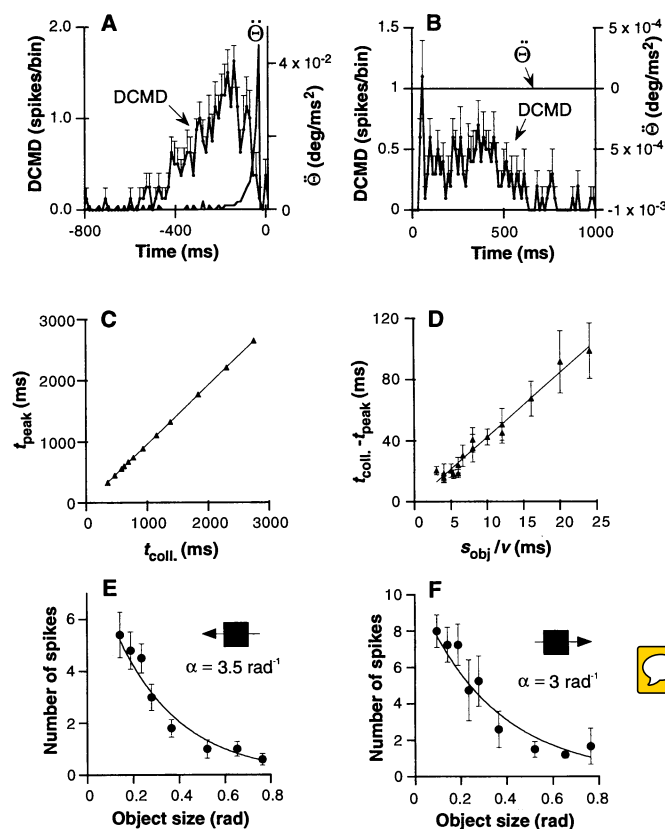
exponential function of the size of the object ($e^{-\alpha\theta}$, where α is positive; Fig. 2, E and F) (18).

The response of DCMD to simulated objects moving toward or away from the eye was then examined (12). In these experiments, both the size and the velocity of the retinal image varied in time, in a manner dependent on the velocity of simulated approach or recession. In all cases tested (3 velocities × 3 sizes = 9 conditions in each of five animals), the response of DCMD at a particular time could be described by a function that simply multiplies the size dependence of its response ($e^{-\alpha\theta}$, as determined above) by the image's instantaneous angular velocity (Fig. 3):

$$f(t) = C|\dot{\theta}(t - \delta)|e^{-\alpha\theta(t - \delta)} \qquad (1)$$

The delay parameter δ represents the latency between the stimulus and DCMD response onsets and was set between 0 and 40 ms (constant value for each animal), as

suggested by experimental evidence (14, 19). C is a proportionality constant (20). $|\dot{\theta}|$ (the absolute value of $\dot{\theta}$) was chosen because DCMD is not directionally selective and thus responds to object recession as well as approach by an increase in firing rate (10, 11). To gain an intuitive understanding of $f(t)$, consider an object approaching at constant velocity v, such that both $\dot{\theta}$ and $e^{\alpha\theta}$ increase with time. When the object is far (θ small), $\dot{\theta}$ increases faster than $e^{-\alpha\theta}$ decreases, resulting in an increase of $f(t)$. As the object approaches, the situation reverses because of the exponential dependence of the last factor in Eq. 1. The function $f(t)$, therefore, peaks before collision.

According to Eq. 1, the time of peak DCMD activity (t_{peak}) relative to the time of collision ($t_{coll.}$) should depend linearly on the ratio of the object size ($S_{obj.}$, Fig. 1A) to the velocity of approach (v), with a slope coefficient of $\alpha/2$ (21):

Fig. 2. Responses of DCMD to moving objects. (**A**) Response of DCMD to a simulated square object ($S_{obj.}$ = 6 cm) approaching at constant velocity (v = 2.5 m/s). Collision would be at time $t_{coll.}$ = 0 ms. DCMD is silent during the first 2000 ms of the 2750 ms of approach. The stimulus, which was limited to the size of the monitor, stopped its expansion at the time indicated by the peak of angular acceleration ($\ddot{\theta}$). However, DCMD activity started to decline about 150 ms before the stimulus peak angular acceleration (that is, while the object was still approaching). Agreement between stimulus angular acceleration and DCMD response (n = 1 animal, 10 trials, bin size = 13.9 ms, mean ± SEM) was poor. (**B**) Response of DCMD to simulated approach of a decelerating square of final size θ = 40°; t = 0 at the onset of approach. Angular acceleration is 0, with angular velocity constant at 31.5 degrees s⁻¹. DCMD fired during more than one-half of the period of approach, and its response profile differed from the acceleration profile of the image (flat). (**C**) Plot of the time of peak DCMD activity (t_{peak}) versus collision time ($t_{coll.}$, relative to the onset of movement). Approach velocity was held constant. Each data point represents a specific combination of object size and approach velocity, averaged over five animals. The standard deviation was too small for display (15). (**D**) Plot of the delay between peak DCMD activity and collision time as a function of $S_{obj.}/|v|$, for four values of v and four object sizes (16 conditions, mean ± SEM, n = 5 animals). Equation 1 predicts that this delay is a linear function of $S_{obj.}/|v|$ with a slope of $\alpha/2$ (21). Data indicate that the relation is indeed linear. The mean value of α (8.59 rad⁻¹), calculated from the slope, is the same as that used to fit the data from one animal in Fig. 3, A to C. (**E** and **F**) Plot of DCMD response (●, total number of spikes per trial), in a different animal, as a function of object size for lateral movement (translation) to the left (E) and to the right (F) at a constant velocity of 3.5π rad s⁻¹ or 625 degrees s⁻¹ (0.4 rad ≈ 23°). Data points (mean ± SD, n = 5 trials) are fitted by the exponential function $e^{-\alpha\theta}$ (18).

Fig. 1. (**A**) Scheme of experimental conditions. θ, angle between the edge of the object [dark square on a bright background (12)] and the focus of expansion; $S_{obj.}$, half-size of the object, or the distance between the focus of expansion and the edge of the object. Movements in depth (d) were simulated on a computer screen by re-creating the changes of the image projected on the retina by an approaching or receding object [θ and $\dot{\theta}$ (12)]. (**B**) Morphology of the LGMD and DCMD (5–7) neurons [adapted from (6)]. The fan-shaped arbor of LGMD is in the lobula (third optic lobe) and receives inputs from small-field, motion-sensitive neurons in the medulla. Branch p is thought to collect feedforward inhibitory inputs from neurons sensitive to wide-field OFF and ON stimuli (8). Arrows indicate the direction of information flow. (**C**) Schematic diagram representing the evolution in time of three functions of θ and $\dot{\theta}$ [$\tau(t)$, $1/\tau(t)$, and $f(t)$] assuming a constant velocity v of approach.

$$t_{coll.} - t_{peak} = \left(\frac{\alpha}{2} \frac{S_{obj.}}{|v|}\right) - \delta \qquad (2)$$

This prediction of linearity was verified experimentally over a wide range of size/velocity ratios in five animals (Fig. 2D). We therefore used the value of α computed for each animal from the slope of the regression line (Eq. 2) to fit the DCMD activity profiles (Fig. 3). The firing rates of DCMD have been superimposed on the values predicted by the model in conditions of constant approach velocity v (Fig. 3, A to C) or constant angular velocity $\dot{\theta}$ (Fig. 3D).

The strength of this model lies in the observation that δ, α, and the exponential dependence on θ were all constrained by
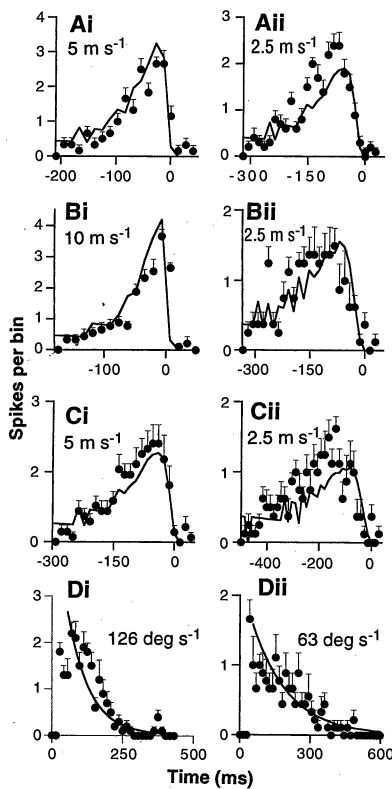

Fig. 3. Test of the model on DCMD response. (**A** to **C**) Response of DCMD (●, mean ± SD, $n = 5$ trials) to approaching squares [$S_{obj.}$ in (A), 3 cm; (B), 4 cm; (C), 6 cm] under conditions of constant approach velocity (v) in one animal. Model prediction [line: $f(t + \delta) = C |\dot{\theta}(t)| e^{-\alpha\theta(t)}$] is superimposed on the data. Irregularities in the model prediction are due to the fact that image velocity and size are calculated from the computer-generated image rather than from theoretical values. Discontinuities are therefore due to image pixelation and refresh and correspond to the exact stimulus seen by the animal. $t = 0$ at collision, $\alpha = 8.59$ rad^{-1}, $\delta = 14$ ms, and $C = 1.22 \times 10^{-3}$. (**D**) Response of DCMD (●, mean ± SD, $n = 5$ trials) in a different animal to approaching squares (final $\theta = 40°$) under conditions of constant angular velocity (simulated deceleration). $t = 0$ at the onset of stimulus. Model prediction [line: $f(t + \delta) = C|\dot{\theta}(t)| e^{-\alpha\theta(t)}$] is superimposed on the data (28). $\alpha = 5.73$ rad^{-1}, $\delta = 42$ ms, and $C = 2.62 \times 10^{-4}$.

independent experimental data and that δ and α were fixed for all size and velocity conditions in each animal (Fig. 3, A to D). In addition, the proportionality constant C used to match the exact values of DCMD firing rates was fixed for all conditions in each animal. Finally, this model also fitted the data obtained with decelerating objects in which the angular velocity of the image edges was held constant (Fig. 3D) (22, 23).

We thus propose a simple algorithm that describes the integrative properties of a visual interneuron and that could, in principle, be used by any visual system to anticipate the time of collision with approaching objects, using simple monocular signals. It has been proposed that whole field inputs to the locust LGMD are provided by feed-forward inhibitory pathways that terminate on a single proximal dendrite (Fig. 1B), separate from the fan-shaped arbor that collects velocity signals from local movement-detector elements (8) [although this proximal dendrite is not present in all LGMD-like neurons (24)]. The good agreement between $f(t)$ and the DCMD response suggests that the dendritic tree of LGMD operates as a biophysical device that multiplies two independent inputs, the size ($e^{-\alpha\theta}$) and velocity ($\dot{\theta}$) signals, during object motion in depth. Using a logarithmic transformation, such multiplication might be accomplished by linear summation of $-\alpha\theta$ (size) and log $\dot{\theta}$ (velocity) and an exponential conversion of the resulting dendritic potential into a firing rate. Alternatively, this multiplication could be performed by way of shunting inhibition (25) of the velocity signal by the size signal on the primary neurite. This neuron may therefore be ideal to study quantitatively the relation between dendritic geometry, intrinsic membrane properties, and computational function. Finally, the principles derived here might be used to design artificial collision anticipation devices, through use of neuromorphic hardware implementations such as silicon retinae (26).

REFERENCES AND NOTES

1. J. J. Gibson, *Psychol. Rev.* **64**, 288 (1957); D. N. Lee, *Philos. Trans. R. Soc. London Ser. B* **290**, 169 (1980); *Perception* **5**, 437 (1976).
2. Y. Wang and B. J. Frost, *Nature* **356**, 236 (1992); H. Wagner, *ibid.* **297**, 147 (1982); M. H. Holmqvist and M. V. Srinivasan, *J. Comp. Physiol. A* **169**, 451 (1991). Other hypotheses for looming detection in flies involve radial expansion–detecting neurons whose outputs feed to a leaky integrator with a long time constant. Landing behavior is evoked when this integrator reaches a certain threshold [A. Borst and S. Bahde, *Naturwissenschaften* **75**, 265 (1988)].
3. D. N. Lee and P. E. Reddish, *Nature* **293**, 293 (1981); D. N. Lee, F. R. van der Weel, T. Hitchcock, E. Matejowsky, J. Pettigrew, *J. Comp. Physiol. A* **171**, 563 (1992).
4. If v is constant, $\tau(t)$ decreases linearly from the onset of approach to the time of collision (Fig. 1C).
5. J. Palka, *J. Insect Physiol.* **13**, 235 (1967); M. O'Shea and J. L. D. Williams, *J. Comp. Physiol.* **91**, 257 (1974).
6. F. C. Rind, *J. Exp. Biol.* **110**, 143 (1984).
7. LGMD or "lobula giant movement detector" neuron (5) receives its inputs in a fan-shaped dendritic tree in the third optic lobe or lobula (Fig. 1B). Each spike in LGMD faithfully triggers a spike in a postsynaptic neuron called "descending contralateral movement detector" or DCMD (5), at frequencies up to 400 Hz (6). DCMD receives no other visual input. Because DCMD activity can easily be monitored extracellularly, we used the response profile of DCMD to visual motion as a monitor of the activity of LGMD, which is the actual wide-field local movement detector neuron. DCMD and LGMD firing rates are thus interchangeable in our experiments.
8. C. H. Rowell, M. O'Shea, J. L. D. Williams, *J. Exp. Biol.* **68**, 157 (1977).
9. G. R. Schlotterer, *Can. J. Zool.* **55**, 1372 (1977).
10. F. C. Rind and P. J. Simmons, *J. Neurophysiol.* **68**, 1654 (1992).
11. P. J. Simmons and F. C. Rind, *ibid.*, p. 1667.
12. Experiments were carried out with 23 adult locusts of either sex; 13/23 were selected for complete analysis. The visual stimuli were programmed on a Hewlett-Packard workstation (HP715/80) with double buffering of screen memory (Starbase graphic library). The images were shown on a video monitor (HP4033A) with a refresh rate of 13.9 ms per frame. The screen, shielded to minimize electromagnetic noise, was placed in the dark, 7 cm in front of one eye; the other eye was masked. Stimuli consisted of one to four dark squares or circles (2 cd m^{-2}) on a bright background (79 cd m^{-2}) that expanded (and then contracted) to simulate approach and recession at constant or variable velocity (for example, mimicking deceleration during approach). The size of the objects on the screen was computed for each frame by perspective projection, with the eye representing the center of projection. At the onset of approach, the objects subtended less than 1° of visual angle, that is, less than the interommatidial angle in the center of the eye. At the end of approach, objects had moved a fixed simulated distance, and the final subtended angle thus varied with the size of the simulated object ($S_{obj} = 3$, 4, 5, and 6 cm). In other trials, the objects moved different distances so that the final value of θ was 40°. Intertrial intervals were 40 or 80 s, to prevent habituation of the response. Data acquisition was synchronized to the stimulus with a photocell that read a marker updated with each image. The activity of DCMD was recorded extracellularly with metal hook-electrodes placed around the neck connectives. The data were stored on digital audio tape and analyzed off-line. Spikes were discriminated digitally (Spikestudio, version 5.1; E. Meir, Cornell University). Peristimulus histograms were constructed with a bin size of 13.9 ms (that is, one bin per stimulus image).
13. This effect has been reported in (10) (figures 7 and 8).
14. The neuron's response lags behind the stimulus, because of neuronal delays. The signal path between stimulus and DCMD response involves phototransduction in the retina, processing in the lamina, medulla, and lobula, and synaptic transmission between LGMD and DCMD. These successive steps probably explain the latency. The exact value of this delay is a function of the intensity and contrast of the stimulus presented, which were kept constant in our experiments (12). Determination of the true value of δ was limited by the resolution with which firing peaks could be measured, that is, by the bin width (13.9 ms), which corresponds to the image refresh rate.
15. The time of DCMD peak firing (t_{peak}) was also strongly correlated with, and preceded, the onset of hindleg femoro-tibial flexion in preparation for an escape jump [flexion onset (in milliseconds) = 19.625 + 1.0038 t_{peak}, $r^2 = 0.9998$]. Five animals were filmed with a video system (60 Hz), and the femorotibial angle was measured with the Peak Movement Analysis System. Synchronization of the video and stimulus signals was achieved with the photocell signal read from the monitor screen (12).
16. Given that acceleration is the second time-derivative of a position signal, it would likely be a very noisy signal to measure and observe accurately.
17. In the case of a translating object, the local edge velocity ω does not correspond to the rate of expansion of the image. By contrast, in the case of an expanding (approaching) object, $\omega = \dot{\theta}$. Although

the stimulus velocity was constant, small variations in the edge velocity may have been perceived by the animal because of the curvature of the eye.

18. The value of α, when measured in conditions of translating and looming stimuli, ranged between 2.9 and 15 rad^{-1} for angular velocities between 314 and 625 degrees s^{-1} in different animals. Single exponential fits were consistently better than linear fits; determination coefficients (r^2) are 0.962 and 0.935 for exponential fits for Figs. 2E (625 degrees s^{-1}) and 2F (-625 degrees s^{-1}) versus 0.850 and 0.835 for linear fits, respectively.
19. M. O'Shea and C. H. Rowell, *J. Exp. Biol.* **65**, 289 (1976).
20. The exact value of C is unimportant; it is not the absolute firing rate that matters, but the fact that the firing rate peaks and then decreases.
21. The function $f(t)$ will peak when its time derivative is 0. From Eq. 1, $df/dt = 0$ if $\ddot{\theta}(t_{peak} - \delta) = \alpha\dot{\theta}^2(t_{peak} - \delta)$. From simple geometrical considerations (Fig. 1A), $\dot{\theta}(t) = (-S_{obj.} v)/(d^2 + S^2_{obj.})$ and $\ddot{\theta}(t) = (2S_{obj.} v^2 d)/(d^2 + S^2_{obj.})^2$. Equation 2, where $t_{coll.}$ is the delay before collision at the start of the movement and t_{peak} is the time when DCMD activity peaks, follows from these three equations.
22. To verify that θ represents the subtended angle of approaching objects and not the angle that separates their

edges from the focus of expansion [point of null velocity during approach or recession (27)], we presented a composite stimulus comprising four squares around the focus of expansion. Each square was one-sixth the size of the ensemble outline. In such conditions, we found that the best fits to the data were obtained when θ represented the angular extent of each object (75% of the variance was explained by model, where C was the only free variable) and not the angle between it and the focus of expansion (14.3% of the variance was explained by model, under the same conditions).

23. It can be shown from Eq. 2 (21) and by using trigonometry that the angle θ_{peak} at which DCMD reaches its peak firing is related to the value of α by the following relation:

$$\cot g\,(\theta_{peak}) = \frac{\alpha}{2} - \frac{|v|\,\delta}{S_{obj.}} \qquad (3)$$

This relation indicates, for example, that if δ or the approach velocity v (or both) are small, the angle θ_{peak} at which the peak firing of LGMD and DCMD is attained should be constant for a wide range of object sizes. Thus, LGMD and DCMD can be considered as preferring a particular and fixed angular size ($\theta_{peak} = \cot g^{-1}\,{}^{\alpha}/_2$). It follows from Eq. 3 that, when δ is not negligible (for example, $\delta = 40$ ms), the peak firing will not occur for a fixed value of θ. When v is constant, for

example, the peak firing will occur earlier if the object is larger. When the object size is held constant, the peak firing will occur later if v is increased.
24. F. C. Rind, *J. Comp. Physiol. A* **161**, 477 (1987).
25. C. Koch and T. Poggio, in *Synaptic Function*, G. M. Edelman, W. E. Gall, W. M. Cowan, Eds. (Wiley, New York, 1987), pp. 637–697.
26. C. Mead and M. Ismael, Eds., *Analog VLSI Implementation of Neural Systems* (Kluwer, Boston, MA, 1989).
27. J. J. Gibson, *The Ecological Approach to Visual Perception* (Houghton Mifflin, Boston, MA, 1979).
28. Note the good agreement between data and model in all size and velocity conditions. Better fits could be obtained if α and δ were unconstrained.
29. We gratefully acknowledge C. Koch (NSF Center for Neuromorphic Systems Engineering) for use of the Hewlett-Packard workstation and D. van Essen for use of the photocell. We thank A. Braun for computer assistance and E. Schuman, C. Koch, and an anonymous referee for comments on the manuscript. Supported by NSF grant IBN-9412426 (F.G.) and an Office of Naval Research grant and NSF–Presidential Faculty Fellow Award to G.L.

■TECHNICAL COMMENTS

Does the p53 Up-Regulated Gadd45 Protein Have a Role in Excision Repair?

Martin L. Smith et al. (1) report stimulation of excision repair in DNA by Gadd45 protein. They used the repair synthesis assay that measures the preferential incorporation of nucleotides into damaged DNA compared to undamaged DNA. As DNA excision repair involves two basic steps, excision and resynthesis, we wished to know whether the increased repair synthesis observed with Gadd45 resulted from increased excision or was a secondary effect of stimulation of the repair polymerase (or polymerases) without actually increasing the amount of adducts removed. We investigated the effects of Gadd45 by the use of the excision assay that measures the release of the damaged nucleotide in the form of an

oligonucleotide (2).

We measured the effect of Gadd45 at various concentrations by the excision assay with HeLa cell-free extracts (Fig. 1). We did not observe any stimulation or inhibition within the concentration range used. As Smith et al. (1) report stimulation of Gadd45
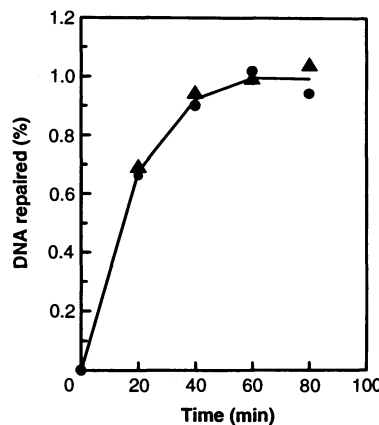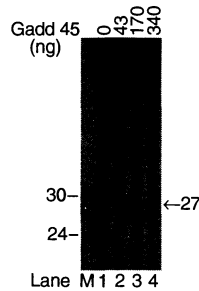
in the range of 40 to 400 ng per assay, we conducted a kinetic experiment using 340 ng of the Gadd45 protein in our standard excision reaction. Gadd45 had no effect on the kinetics of excision repair (Fig. 2).

To eliminate the possibility of experimental artifacts resulting from nonrepair proteins in cell-free extracts that can bind to Gadd45 and interfere with its repair stimulatory effect, we also tested the effect of Gadd45 protein on repair, with the use of a defined excision nuclease system reconstituted from highly purified repair proteins (2). We saw no effect on excision repair in this system with the concentration of Gadd45 tested. We considered that the stimulatory effect could be unique to the cell lines used by Smith et al. (1). Therefore, we performed the excision assay with the ML-1 cell line used by Smith et al. (1). The cell-free extract from this cell line gave a weaker excision signal compared to HeLa cell-free extract; however, as with HeLa cell-free extract and with the defined system, Gadd45 did not have a stimulatory effect on excision by the ML-1 cell-free extract (Fig. 3).

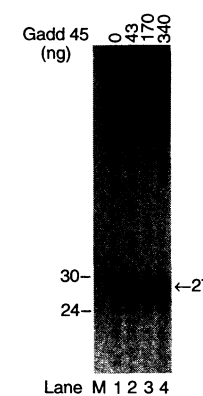As Smith et al. (1) used the repair synthesis assay, and as they found that Gadd45

Fig. 1. Effect of Gadd45 on DNA repair by HeLa cell-free extract as measured by the excision assay. HeLa cell-free extract (50 μg) was supplemented with the indicated amounts of Gadd45 protein, and excision reaction was carried out under standard conditions (5) for 60 min. Human excinuclease excised the lesion in 25- to 27-nucleotide-long oligomers (6), which were resolved on 10% denaturing polyacrylamide gels. Lane M contains 30- and 24-nucleotide-long oligomers used as size markers. Arrow indicates the major excision product.

Fig. 2. Effect of Gadd45 on the kinetics of DNA excision repair with HeLa cell-free extracts. HeLa cell-free extracts (50 μg) were supplemented with 340 ng of Gadd45 protein, and the excision assay was carried out for the indicated times. The products were analyzed on a 10% denaturing polyacrylamide gel. The level of repair was determined by analysis of the excision gels using PhosphorImager (Molecular Dynamics, Sunnyvale, California). Data points are averages of two experiments. Circles, without Gadd45; triangles, with Gadd45.

Fig. 3. Effect of Gadd45 on excision repair with ML-1 cell-free extracts. Indicated amounts of Gadd45 protein were added to ML-1 cell-free extracts (50 μg) and excision assay was performed under standard conditions (5).